Coronavirus nsp10/nsp16 methyltransferase can be targeted by nsp10-derived peptide in vitro and in vivo to reduce replication and pathogenesis

Running title: Peptide TP29 inhibits MHV replication

Yi Wang[1¶], Ying Sun[2¶], Andong Wu[1], Shan Xu[1], Ruangang Pan[1], Cong Zeng[1], Xu Jin[1], Xingyi Ge[3], Zhengli Shi[3], Tero Ahola[4], Yu Chen[1]#, Deyin Guo[1]#

[1] State Key Laboratory of Virology, College of Life Sciences, Wuhan University, Wuhan, China.

[2] Department of Pathogen Biology, Henan University of TCM, Zhengzhou, China.

[3] Center for Emerging Infectious Diseases, State Key Laboratory of Virology, Wuhan Institute of Virology, Chinese Academy of Sciences, Wuhan, China.

[4] Department of Food and Environmental Sciences, University of Helsinki, Helsinki, Finland.

#Address correspondence to Deyin Guo, dguo@whu.edu.cn

#Address correspondence to Yu Chen, chenyu@whu.edu.cn

[¶]These authors contributed equally to this work.

Word count abstract: 232 (abstract), 149 (importance)

Word count text: 8,961

Abstract

The 5' cap structures of eukaryotic mRNAs are important for RNA stability and protein translation. Many viruses that replicate in the cytoplasm of eukaryotes have evolved 2'-*O*-methyltransferases (2'-*O*-MTase) to autonomously modify their mRNAs and thus carry a cap-1 structure (m7Gppp-Nm) at the 5'-end, thereby facilitating viral replication and escaping innate immune recognition in host cells. Previous studies showed that the 2'-*O*-MTase activity of severe acute respiratory syndrome coronavirus (SARS-CoV) non-structural protein 16 (nsp16) needs to be activated by nsp10 whereas nsp16 of feline coronavirus (FCoV) alone possesses 2'-*O*-MTase activity. In this study, we demonstrate that stimulation of nsp16 2'-*O*-MTase activity by nsp10 is a universal and conserved mechanism in coronaviruses including FCoV and that nsp10 is functionally interchangeable in stimulation of nsp16 of different coronaviruses. Based on our current and previous studies, we designed a peptide (TP29) from the sequence of the interaction interface of mouse hepatitis virus (MHV) nsp10 and demonstrated that the peptide inhibits the 2'-*O*-MTase activity of different coronaviruses in biochemical assays and the viral replication in MHV infection and SARS-CoV replicon models. Interestingly, the peptide TP29 exerted robust inhibitory effects in vivo in MHV infected mice by impairing the MHV virulence and pathogenesis through suppressing virus replication and enhancing type I interferon production at an early stage of infection. Therefore, as a proof-of-principle, the current results indicate that coronavirus 2'-*O*-MTase activity can be targeted in vitro and in vivo.

Importance

Coronaviruses (CoVs) are important pathogens of animals and human with high zoonotic potential. SARS-CoV encodes the 2'-*O*-methyltransferase (2'-*O*-MTase) that is composed of the catalytic subunit nsp16 and the stimulatory subunit nsp10, and plays an important role in virus genome replication and evasion from innate immunity. Our current results demonstrate that stimulation of nsp16 2'-*O*-MTase activity by nsp10 is a common mechanism for coronaviruses. And nsp10 is functionally interchangeable in the stimulation of nsp16 among different coronaviruses, which underlies the rationale for developing inhibitory peptides. We demonstrate that a peptide derived from the nsp16-interacting domain of mouse hepatitis virus (MHV) nsp10 could inhibit 2'-*O*-MTase activity of different coronaviruses in vitro and viral replication of MHV and SARS-CoV replicon in cell culture. And it could strongly inhibit virus replication and pathogenesis in MHV-infected mice. The work makes it possible to develop broad-spectrum peptide inhibitors by targeting the nsp16/nsp10 2'-*O*-MTase of coronaviruses.

Introduction

The 5'-ends of eukaryotic cellular mRNAs and most viral mRNAs possess a cap structure, which plays important roles in mRNA splicing, intracellular RNA transport, RNA stability and translation initiation (1). Host and viral RNA molecules lacking the 5'-cap structure are rapidly degraded in the cytoplasm (2). The cap-0 structure of mRNA is co-transcriptionally formed through sequential enzymatic reactions including RNA triphosphatase (TPase), RNA guanylyltransferase (GTase) and RNA (guanine-N7)-methyltransferase (N7-MTase) (1). In higher eukaryotes and some viruses, cap-0 structure m7GpppN-RNA is further methylated at the ribose 2'-*O* position of the nascent mRNA by a ribose 2'-*O*-methyltransferase (2'-*O*-MTase) to form cap-1 structure (m7GpppNm) and cap-2 structure (m7GpppNmNm). Both N7-MTase and 2'-*O*-MTase can catalyze the transfer of the methyl group from the methyl donor S-adenosyl-L-methionine (SAM or AdoMet) to RNA substrate and generate S-adenosyl-L-homocysteine (SAH or AdoHcy) as a by-product. The functions of viral RNA cap structure include: (i) the guanosine cap core structure protects the 5'-triphosphate from activating the host innate immune response (3, 4); (ii) the N7-methylation is essential for viral replication through the enhancement of viral RNA translation (5); and (iii) the 2'-*O* methylation functions to evade the recognition of host RNA sensors such as RIG-I, Mda-5, and IFIT and to resist the interferon (IFN) mediated antiviral response (6, 7). Since many RNA viruses replicate in the cytoplasm, they cannot access the host capping machinery located in the nucleus. Therefore, most of them have evolved to encode their own capping apparatus. The critical role of viral

RNA cap structure and the distinct mechanisms of host and viral RNA capping formation have opened new opportunities for vaccine and antiviral drug development (8, 9).

Coronaviruses (CoVs) are common pathogens of respiratory, gastrointestinal, hepatic and central nervous systems diseases of humans and animals (10). It has been reported that bats are natural carriers of coronaviruses (11-13) and that coronaviruses may be transmitted from animals to humans as exemplified by severe acute respiratory syndrome coronavirus (SARS-CoV) and Middle East respiratory syndrome coronavirus (MERS-CoV) (14). Therefore, coronaviruses are important pathogens that threaten human health and economy. The *Coronavirinae* subfamily is classified into four genera, including *alphacoronavirus, betacoronavirus, gammacoronavirus and deltacoronavirus* (15). The classification was originally based on antigenic relationships and later confirmed by sequence comparisons of entire viral genomes (16). Coronaviruses are enveloped, positive-sense single-stranded RNA viruses. The 5'-terminal two thirds of the coronaviral genome contains a large open reading frame ORF1ab, which encodes polyprotein 1a (pp1a) and polyprotein 1ab (pp1ab), the latter being generated via a -1 ribosomal frameshift (17). The polyproteins pp1a/1ab are cleaved into 16 nonstructural proteins (nsp1 to nsp16) including many RNA processing enzymes such as RNA-dependent RNA polymerase (nsp12) (18, 19), RNA helicase and triphosphatase (nsp13) (20), exoribonuclease and N7-MTase (nsp14) (21-23), endonuclease (nsp15) (24) and 2'-*O*-MTase (nsp16) (25-28).

In previous studies, we and others have identified nsp14 and nsp10/16 complex of

Journal of Virology

105 SARS-CoV as respective N7-MTase and 2'-*O*-MTase, both of which are involved in
106 viral RNA methylation and formation of the cap-1 structure (23, 25-28).
107 Structure-function analysis of SARS-CoV nsp14 revealed the characteristics of this
108 novel N7-MTase that is associated with exoribonuclease activity in the same protein
109 (29). Interestingly, nsp10 acts as the stimulatory factor for nsp16 by stabilizing the
110 SAM-binding pocket and extending the substrate RNA-binding groove of nsp16 as
111 revealed by crystallographic and biochemical studies (28). Interference of the
112 interaction between nsp10 and nsp16 of SARS-CoV by short peptides could
113 specifically inhibit the activity of 2'-*O*-MTase (30). However, nsp16 of feline
114 coronavirus (FCoV) from the genus *alphacoronavirus* was shown to methylate the
115 cap-0 structure at the ribose 2'-*O* position of the first nucleotide of viral RNA to form
116 cap-1 structure in the absence of nsp10 (25). Therefore, it remains unclear whether the
117 stimulatory effect of nsp10 on nsp16 methyltransferase is universal for all
118 coronaviruses. Therefore, further studies on the mechanisms and characteristics of the
119 2'-*O*-MTase of different coronaviruses will benefit the development of antiviral
120 inhibitors that specifically targeting coronaviral 2'-*O*-MTase.

121 In this study, we provide evidence that stimulation of nsp16 methyltransferase activity
122 by nsp10 is a common mechanism for coronaviruses although FCoV nsp16 alone
123 possesses a low 2'-*O*-MTase activity. We further demonstrate that nsp10 is
124 interchangeable in the stimulatory function among different coronaviruses, and a
125 peptide derived from the conserved interaction domain of MHV nsp10 shows
126 broad-spectrum inhibitory effect on 2'-*O*-MTase activity *in vitro* and virus replication .

Journal of Virology

These results have implications for designing specific anti-coronaviral drugs to control the viral infection.

Materials and Methods

Protein expression and purification

The coding sequences of nsp16 and nsp10 from SARS-CoV, MHV, TGEV and FCoV were PCR amplified from cDNAs of the SARS-CoV WHU strain (GenBank accession no. AY394850), MHV-A59 (GenBank accession no. AY700211.1), TGEV (GenBank accession no. FJ755618.2) and FCoV (GenBank accession no. AJ311317.1). The cDNAs of MERS-CoV nsp16 and nsp10 were chemically synthesized according to the deposited sequence of MERS-CoV (GenBank accession no. KF192507.1). The cDNAs of nsp16 or nsp10 of SARS-CoV or MHV-A59 was inserted into the NdeI and SalI sites of the vector pET30a using standard recombinant DNA techniques. The coding sequence of nsp16 or nsp10 of TGEV (kindly provided by Dr. Luis. Enjuanes), FCoV (kindly provided by Dr. Peter J. M. Rottier) and MERS-CoV was cloned into the BamHI and XhoI sites of pET30a, resulting in addition of 30 extra amino acid residues at their N-terminus. The plasmid for IBV expression (pDest14-IBV-nsp16 and pDest14-IBV-nsp10) was a kind gift from Dr. Eric J. Snijder.

All expression plasmids separately transformed into *E. coli* BL21 (DE3) cells (Novagen) that were cultured at 37°C in 1 liter of Luria-Bertani (LB) medium with 50 μg/ml kanamycin or 100 μg/ml ampicillin and then induced with 0.4 mM isopropyl-β-D-1-thiogalactopyranoside (IPTG) at 16°C for 12 hours. The purification

149 of nsp16 and nsp10 with His-Tag of SARS-CoV, MHV-A59, MERS-CoV, TGEV,
150 IBV and FCoV were performed as described previously (28).

151 **Preparation of RNA substrates**

152 ATP- and UTP-initiated RNA substrates comprising 20 nucleotides ($pppAC_{20}$
153 and$pppUC_{20}$) were in vitro transcribed and purified as previously described (23, 28).
154 Unlabeled cap-0 structure m7GpppA-RNA was prepared from transcribed RNA
155 (pppA-RNA) by vaccinia virus capping enzyme (D1/D12) following the
156 manufacturer's protocol (Epicentre). The ^{32}P-labeled cap structures
157 (m7G*pppA-RNA) used as RNA substrates and cap analogues (G*pppA, m7G*pppA
158 and m7G*pppAm) used as positive controls were prepared and purified as previously
159 described (23, 29).

160 **Biochemical assays for MTase activity**

161 The MTase activity analyses were performed by thin layer chromatography (TLC)
162 using ^{32}P-labeled RNA substrates or by liquid scintillation assays after purification of
163 the ^{3}H-labeled substrates with DEAE-Sephadex chromatography as previously
164 described (28, 29, 31). The protocol of the MTase assay is also available in the
165 Bio-protocol (http://www.bio-protocol.org/).

166 **Peptide synthesis**

167 Based on the crystal structure and our previous study (30), short peptides (Table 1)
168 were synthesized (Shanghai Ji'er Biochemistry) with N-terminal acetyl and
169 C-terminal amide modifications. The N-termini of TP29 (Tat-P29), TP29S
170 (Tat-Scramble) and TP29M (Tat-P29-R93A & F96A) were fused with HIV

Tat-derived peptide (YGRKKRRQRRRGSG) to increase the cell-penetrating capability of peptides. All of the peptides were purified by HPLC and verified by mass spectrometry. The peptides were dissolved in phosphate buffer saline (PBS) before use.

Cell, viruses and mice

Rat lung epithelial cells (L2) and wild-type MHV-A59 were kindly provided by Dr. Rong Ye (Shanghai Medical School of Fudan University). L2 cells, Baby hamster kidney cells (BHK-21) and Vero E6 cells were grown in DMEM (GIBCO, Invitrogen) supplemented with 10 % fetal bovine serum (FBS). Virus-free C57BL/6 mice were obtained from the Center for Disease Control and Prevention of Hubei province (Wuhan, China). All mice were maintained in individually ventilated cages in bio-safety level 2 (BSL2) facilities and received care in compliance with international legal requirements throughout the experiments. Intrahepatic inoculations were carried out under anesthesia with 4 % chloral hydrate and all efforts were made to minimize suffering.

Cell viability, peptide inhibition and luciferase activity assays

Cell viability of L2, BHK-21 and Vero E6 cells in 96-well plates was assessed 16 hours after peptide was added by Cell Counting Kit-8 (CCK8) (Dojindo). Cell culture in each well was added with 10 μl of CCK-8 solution (WST-8 [2-(2-methoxy-4-nitropheny)-3-(4-nitrophenyl)-5-(2,4-disulfophenyl)-2H-tetrazolium, monosodium salt]), which specifically stained the living cells, by following the manufacturer's protocol.

L2 cells were infected with viruses at a multiplicity of infection (MOI) of 0.1 and incubated at 33°C for 1 hour. Infected cells were washed three times with 2 mL of DMEM and supplied with peptide at the final concentration of 200 μM in pre-warmed 10 % FBS-DMEM. Cells were then incubated at 33°C and the virus was collected at 20 hours post infection. Virus titers were determined by Virus Counter (Virocyt Virus Counter 2100) and plaque assays. For measurement with the Virus Counter, virus in cell culture was collected at room temperature, centrifuged at 14,000 rpm for 10 min and then the supernatant was added in Sample Dilution Buffer with 1:10 dilution. Subsequently, in the process of staining, Combo Dye was mixed with the sample at a ratio of 1:2 and incubated in dark for 30 min at room temperature. The number of virus particles was determined following the manufacturer's protocol.

BHK-21 cells were transfected with Rep-SCV-luc/neo reporters (180 ng) together with pRL-TK (50 ng, as transfection efficiency control) with FuGENE HD Transfection Reagent (Roche Applied Science) according to the manufactturer's instruction. The peptides were added to the culture medium at the final concentration of 200 μM at 1 hour post transfection. The cells were collected and lysed at 20 hours post transfection (32), and then subjected to luciferase activity assays by using the Dual-Glo System (Promega, Madison, WI) following the manufacturer's protocol.

Viral infection of mice, histological analysis and alanine aminotransferase (ALT) measurements

Groups of three-week old mice were infected by intrahepatic (i.h.) inoculation with MHV-A59 diluted in PBS containing 0.75 % bovine serum albumin or an equal

volume of uninfected cell preparation (mock infection) at a comparable dilution. Liver tissues were harvested at the indicated days post infection. The tissues were cut into blocks and fixed in phosphate buffered 4 % paraformaldehyde, pH 7.4, for tissue embedding, or frozen in PBS with 0.167 % gelatin for titering of infectious virus (33). For the homogenization, livers were soaked in chilled PBS and ground in a tissue homogenizer (OSE-Y20, TIANGEN) at 4°C with 20 volumes of PBS. The homogenates were centrifuged for 10 min at 400× g and the supernatant kept at -20°C until use. Standard plaque assays were performed on L2 cells as described previously (34).

For the measurement of the inhibition of peptides on the virus replication in mouse, groups of mice were infected by intrahepatic (i.h.) inoculation with 500,000 PFU of MHV-A59 and then the peptide (TP29, TP29M or TP29S) at the final concentration of 0.5 mg/g or PBS (non-treatment control) were injected intrahepatically. Mice for each test group were sacrificed at days 1, 3, 5 and 7 post infection, respectively, and the livers were removed and placed directly into 2 ml of isotonic saline with 0.167 % gelatin, weighed, and stored frozen at -70°C until use.

For the measurement of alanine aminotransferase (ALT)/glutamic-pyruvic transaminase (GPT) levels, blood was incubated with serum accelerator at room temperature to allow coagulation, and was then centrifuged to obtain serum; the serum was used for measurements of ALT levels using an ALT/GPT kit (NJJCBIO, C009-2).

Journal of Virology

Results

Stimulation of the 2'-O-MTase activity of nsp16 by nsp10 is a common mechanism for coronaviruses

Previous studies have revealed that FCoV nsp16 alone possesses 2'-*O*-MTase activity but SARS-CoV nsp16 requires the stimulation of nsp10 (25-28). To address this disparity and test whether the nsp10 from other coronaviruses displays stimulatory function, we characterized the 2'-*O*-MTase activity of representative viruses from three coronavirus genera: transmissible gastroenteritis virus (TGEV) and FCoV from *alphacoronavirus*; mouse hepatitis virus (MHV) from lineage A of *betacoronavirus*; SARS-CoV from lineage B of *betacoronavirus*; MERS-CoV from lineage C of *betacoronavirus*; and infectious bronchitis virus (IBV) from *gammacoronavirus*. The recombinant nsp10s and nsp16s of these coronaviruses were expressed and purified, and SDS-PAGE analysis showed that the purity of the recombinant proteins was more than 95 % with the expected molecular mass (Fig. 1A). As different cloning sites were used, the nsp16 and nsp10 of TGEV, FCoV and MERS-CoV contain 30 additional amino acid residues at their N-terminus, leading to slower mobility than that of SARS-CoV, MHV and IBV (Fig. 1A) but no activity reduction (Figures 1B-1H). The biochemical assays were performed to measure the MTase activity of each nsp16 in the presence or absence of the corresponding nsp10 using cap-0 RNA (m7GpppA-RNA) and ^{3}H-labeledS-adenosyl [methyl-^{3}H] methionine as substrates. SARS-CoV nsp7 and vaccinia virus (VV) VP39, the latter representing a well characterized 2'-*O*-MTase, were used as negative and positive control, respectively.

As shown in Fig. 1, nsp10 or nsp16 alone of all the coronaviruses, except FCoV nsp16 (Fig. 1C), did not show 2'-*O*-MTase activity. FCoV nsp16 alone showed a low but detectable MTase activity, which is consistent with a previous report (25). In contrast, in the presence of the corresponding nsp10, the nsp16s of TGEV (Fig. 1B), MHV (Fig. 1D), SARS-CoV (Fig. 1E), MERS-CoV (Fig. 1F) and IBV (Fig. 1G) were activated and showed robust MTase activities. Although the nsp16 of FCoV alone could methylate the RNA substrate to certain extent, its MTase activity was increased more than 3 fold in the presence of nsp10 (Fig. 1C). These results clearly indicate that the stimulation of nsp16 MTase activity by nsp10 is a common mechanism for coronaviruses including FCoV. To further confirm the position of methylation on the RNA substrates, the cap-0 m7G*pppA-RNA (where * indicates that the following phosphate was ^{32}P-labeled) was treated with nsp16 or nsp10/nsp16 complex of all selected coronaviruses. The methylated RNAs were digested with nuclease P1 that cleaves capped RNAs into 3'-OH-terminated cap structures and 5'-pN_{OH}. The resulting cap structures were analyzed by thin layer chromatography (TLC). As expected, the P1 cleavage products of RNA treated with nsp10/nsp16 complex co-migrated with m7G*pppAm, the cap-1 structure (Fig. 1H). In contrast, the cleavage products treated by the nsp16 alone remained as cap-0 structure m7G*pppA, except for FCoV nsp16 treatment, which generated a small fraction of products that co-migrated with m7G*pppAm structure (Fig. 1H).

Although structural analysis shows that nsp10 and nsp16 stay at the ratio of 1:1 in the nsp10/nsp16 complex of SARS-CoV (27, 28), the nsp10 is translated 3 to 5 times

more than nsp16 in the infected cells (35, 36). Therefore, we investigated whether the physiological surplus of nsp10 plays a role in the enzymatic activity of nsp16, especially for FCoV nsp16. As shown in Fig. 2, nsp10 could significantly increase the enzymatic activity of coronavirus nsp16 in dose-dependent manner, including FCoV nsp16. The ratio of nsp16 to nsp10 for maximal enzymatic activity of FCoV 2'-*O*-MTase is 1:3; while it is around 1:8 for other coronaviruses, although the MTase activities did not significantly increase from 1:6. This is consistent with the physiological ratio of nsp16 to nsp10 in infected cells. Therefore, the ratio 1:6 of nsp16 to nsp10 was used in the following biochemical assays to mimic the physiological environment of coronaviral infection.

The nsp10s of coronaviruses are interchangeable in stimulating the nsp16 2'-*O*-MTase activity among coronaviruses

In previous studies, the crystal structure of SARS-CoV 2'-*O*-MTase revealed the critical residues involved in the interaction between nsp10 and nsp16, which might contribute to the binding of cofactor SAM (such as Lys93 of nsp10 with Ser105 of nsp16) (28) and RNA substrates (such as Tyr96 of nsp10 with Gln87, Arg86, Ala83 and Val84 of nsp16), respectively (27, 28, 37). Although alignments of primary sequences of both nsp10 (Fig. 3A) and nsp16 (Fig. 3B) of coronaviruses showed the similarity of approximate 40 %, the identified critical residues on the interaction interface of nsp10 and nsp16 of SARS-CoV are highly conserved among coronaviruses (Figs. 3A and 3B). Therefore, we assumed that the nsp10 of one coronavirus might be able to stimulate the nsp16 2'-*O*-MTase of another virus. To test

this assumption, we first analyzed whether nsp10 was interchangeable among the coronaviruses of the same genus. As shown in Figs. 3C and 3D, the MTase activities of nsp16 could be stimulated efficiently by any other nsp10 from the same genus to the similar level. We further analyzed the stimulatory effect of nsp10 from coronaviruses of different genera. As shown in Fig. 4, the nsp16 of TGEV could be fully stimulated by the nsp10 of *alphacoronavirus* and less efficiently activated when using the nsp10 of *betacoronavirus* and *gammacoronavirus* (Fig. 4A). In contrast, the FCoV nsp16 could be stimulated to similar level either by cognate nsp10 or non-cognate nsp10s (Fig. 4B), which may reflect the fact that FCoV nsp16 alone already possesses a certain degree of MTase activity (Fig. 1C) and thus indicates that it may be further stimulated more efficiently by an nsp10 of any coronavirus. Interestingly, nsp16s of *betacoronavirus*, including MHV (Fig. 4C), SARS-CoV (Fig. 4D) and MERS-CoV (Fig. 4E), could be fully activated and stimulated with the help of nsp10s of all selected coronaviruses from different genera. In contrast, the nsp16 of IBV (*gammacoronavirus*) was only activated and stimulated remarkably by its cognate nsp10 (Fig. 4F). Taken together, these results indicate that the characteristics of coronavirus nsp10 and nsp16 might vary, but the mechanisms of 2'-*O*-MTases stimulated by nsp10s are relatively conserved. Moreover, the nsp10s of different coronaviruses may share some critical residues for binding nsp16s and they are functionally interchangeable among different coronaviruses.

Development of a broad-spectrum peptide inhibitor against coronaviral 2'-*O*-MTase

The conserved mechanism and interchangeability of nsp10 in the activation and stimulation of coronaviral 2'-*O*-MTases provides a possibility to develop broad-spectrum inhibitors for repressing the 2'-*O*-MTase activities of different coronaviruses. In previous studies, we showed that the region of amino acids (aa) 65-107 of nsp10 is sufficient for the interaction with nsp16 but unable to stimulate the 2'-*O*-MTase activity while peptides derived from this region could suppress nsp16 activity in vitro (30). In this study, we designed a peptide that corresponds to aa 68-96 of MHV nsp10 and tested its inhibitory effects in the replication models of MHV and SARS-CoV replicon. Two residues (the basic K93 and aromatic Y96) of SARS-CoV nsp10 were shown to be critically involved in the interaction with nsp16 (27, 28, 37) and are well conserved in nsp10 of different coronaviruses, where the lysine can be replaced by arginine (R) and tyrosine by phenylalanine (F) (Fig. 3A, marked by open triangles). To confirm that these two residues are important for the stimulatory function of nsp10, recombinant nsp10s of 6 coronaviruses with either K/R to A or Y/F to A mutation were expressed, purified and tested in MTase activity assays. As shown in Fig. 5A, when either of the two critical residues was changed to alanine, the stimulatory function of nsp10 was largely disrupted, indicating that the two residues are essential for stimulating nsp16 activity. To test the inhibitory effect of MHV nsp10-derived peptide on nsp16 of different coronaviruses, we chemically synthesized three peptides: P29 (aa 68-96 of MHV), P29M (P29 sequence with mutations of the critical residues, R93A and F96A), and P29S (with scrambled sequence of P29) (Table 1). P29M and P29S were used as negative controls in the assays. The peptides were added to the mixture of nsp16s and nsp10s in the MTase assays. As shown in Fig. 5B, comparing with P29M and scrambled peptide P29S, P29 could significantly inhibit the MTase activity of nsp16s of MHV, SARS-CoV, MERS-CoV and IBV by

more than 50 % inhibitory efficiency, and modestly repress that of nsp16s of *alphacoronavirus* (TGEV and FCoV). These results indicate that the peptide P29 derived from the interaction domain of MHV nsp10 possesses a broad-spectrum inhibitory activity on nsp10/nsp16 complex of a number of different coronaviruses in the *in vitro* assays.

Inhibition of coronavirus replication by P29 in cell culture models

Next we tested whether the peptide P29 could inhibit virus replication in the replication models of MHV live virus and SARS-CoV replicon. To deliver the short peptide to cells, the N-terminus of peptides P29, P29M and P29S was fused with a short peptide from HIV-Tat (YGRKKRRQRRRGSG), which is arginine-rich and can act as cell-penetrating carrier to deliver the cargo to cytosol and nucleus (38). The HIV-Tat fused peptides were named as TP29, TP29M and TP29S, respectively (Table 1). To evaluate the cytotoxicity of the Tat fused peptides, cell viability was tested by CCK-8 assays, which showed that they were well tolerated by baby hamster kidney cells (BHK-21), Vero E6 cells and rat lung epithelial cells (L2) at final concentrations 20~400 μM and no cytotoxicity was observed (data not shown).

We first tested the inhibitory effects of P29 on MHV replication. L2 cells were infected with MHV-A59 at a multiplicity of infection (MOI) of 1. 1 hour after infection, peptides TP29, TP29M, P29 and TP29S were added to the culture medium at the final concentration of 200 μM. Virus titers were measured (Fig. 6A) and further verified by plaque assays (Fig. 6B) 20 hr post infection. TP29 reduced the titer of MHV-A59 by 80 %in comparison with the mock control (PBS), while TP29M, TP29S and P29 did not display significant inhibitory effects (Figs. 6Aand 6B). Notably, the peptide P29 showed inhibitory activity in the *in vitro* assays (Fig. 5B) but not in cell cultures, indicating that the fused HIV-Tat peptide is essential for the delivery of the

peptides into cells. Moreover, the average diameter of viral plaque with TP29 treatment was two times smaller than that with TP29S 20 hours post infection (Fig. 6C), which indicates that TP29 slowed down the growth of MHV-A59. The dose-response curve of TP29 showed that the inhibitory concentration of 50 % (IC50) value against MHV is approximately 60 μM (Fig. 6D).

We then tested the capacity of the peptides TP29, TP29M and TP29S to inhibit the replication of SARS-CoV replicon (Rep-SCV-luc/neo), which harbors the firefly luciferase reporter gene under the control of M gene transcription regulatory sequence (TRS) (32). Renilla luciferase was employed as a transfection control. The peptides were added to the culture medium at the final concentration of 200 μM, 1 hour post co-transfection of Rep-SCV-luc/neo and Renilla luciferase in BHK-21 cells. As shown in Fig. 6E, comparing with TP29M and TP29S, TP29 repressed the replication of SARS-CoV replicon by 50 %. Together, these results suggest that peptide TP29 could suppress the replication of different coronaviruses in cell cultures, consistent with its broad-spectrum activity observed in the *in vitro* assays.

Peptide TP29 can rescue MHV-infected mice by inhibiting viral replication and enhancing the IFN response

We further tested whether peptide TP29 could inhibit virus replication *in vivo* in an animal model. C57BL/6 mice (n = 10) were infected by intrahepatic (i.h.) inoculation with 500,000 PFU of wild-type MHV-A59 or an equal volume of uninfected cell preparation (mock infection) at a comparable dilution. The peptides (TP29 or TP29S) at a final concentration of 0.05 mg/g (the amount of peptide to the body weight of mice) or PBS were intrahepatically injected immediately post infection (p.i.) of

MHV-A59, respectively. The survival percentage (%) of each group (mock infection and MHV infection with TP29, TP29S and PBS) was statistically analyzed during the 14-day observation period (Fig. 7A). The MHV infected mice supplied with TP29S and PBS began to die at day 4 p.i., and all of them (10/10) died 7 days post infection (Fig. 7A). However, all (10/10) of the infected mice treated by TP29 and the mice inoculated with uninfected cell preparation (mock infection) survived (Fig. 7A), which exceeds the expectations considering its inhibitory effect in cell culture models (Fig. 6). To evaluate the effects of TP29 on virus replication and pathological changes, C57BL/6 mice (n = 7) were infected with MHV-A59 as described above, and intrahepatically injected with peptides or PBS (mock control) immediately (0 hour) or 1 hour post infection, respectively. The mice were sacrificed at day 3 post infection and viral titers in livers (Fig. 7B) and serum alanine aminotransferase (ALT) values (Fig. 7C) of each group were analyzed. Interestingly, with the protection of TP29 at or after infection, the virus titers of MHV infected mice livers sharply decreased by 1.5 $\log_{10}$ (Fig. 7B), and the serum ALT values, which indicate the damage level of liver cells caused by the virus-induced acute hepatitis in clinical diagnosis (39), were 10 times less than that of other groups (Fig. 7C). Moreover, the intrahepatic injection of the peptides showed no side effects to hosts as the ALT values in mock infection controls remained at background level (Fig. 7C). These results demonstrated that the inhibitory efficacy of TP29 *in vivo* is significantly higher than in cell cultures (Fig. 6), which implies that an additional antiviral mechanism such as innate immunity might be enhanced beside the direct inhibitory effect of TP29 on the nsp16 MTase activity.

The nsp16 2'-*O*-MTase activity has been shown to play an important role in the evasion of innate immunity and deficiency in the 2'-*O*-MTase may lead to increased IFN responses against virus infection (6, 7). Therefore, we further tested whether TP29 treatment could increase IFN production during MHV infection and analyzed IFN-β levels as well as serum ALT values in the MHV-infected C57BL/6 mice (n = 7) treated by TP29, TP29S (scrambled TP29) or PBS, respectively. In addition, one group of mice was treated with TP29 but not infected with MHV. The mice were sacrificed 1, 3, 5 and 7 days post infection. As shown in Fig. 7D and 7E, the serum IFN-β levels of TP29-treated mice were significantly enhanced 24 hours post infection while the virus titer was 1.5 $\log_{10}$ times lower than that in TP29S-treated mice (Fig. 7D). The treatment with TP29 without MHV infection did not enhance IFN-β production in mice (Fig. 7D). In contrast, the serum IFN-β levels of TP29S treated mice sharply increased to 115 pg/ml 72 hours (3 days) post infection (Fig. 7D). Accordingly, the viral titers of TP29S-treated mice kept increasing and were finally killed 6 days post infection (Fig. 7E). The kinetics of serum ALT values showed that the livers of TP29 treated mice were well protected at day 3 post infection and the ALT values began to decrease 7 days post infection (Fig. 7F). These phenomena were also verified by pathological section analysis of mice livers stained with hematoxylin and eosin. As shown in Fig. 7G, the number and size of the foci of hepatocyte necrosis, inflammatory cells and lymphocytic infiltration, which represent acute hepatitis in the liver parenchyma, were significantly smaller in TP29-treated mice than in other groups; the liver of the former was restored to a normal state 7 days post infection.

442 Taken together, these results indicate that the peptide TP29 could rescue
443 MHV-infected mice by inhibiting viral replication and inducing the IFN response at
444 the early stage of infection. Therefore, the increase of IFN response by TP29
445 treatment may have contributed to the potent inhibition of virus replication and
446 pathogenesis of MHV infection.

447 **Discussion**

448 Coronaviruses belong to the largest RNA viruses and form a complicated
449 replication/transcription complex (RTC), which is composed of 16 non-structural
450 proteins (nsps) and some unknown host factors (40, 41). A number of nsps have been
451 identified as RNA processing/modification enzymes, among which nsp14 is an
452 exoribonuclease/N7-(guanine)-methyltransferase (21-23) and nsp16 is a 2'-*O*-MTase
453 (25-28). In the previous studies, it has been shown that SARS-CoV nsp16 exerts the
454 2'-*O*-MTase activity only in the presence of nsp10 whereas FCoV nsp16 alone
455 possesses the 2'-*O*-MTase activity to some degree (25-28). In this study, we
456 demonstrated that stimulation of the nsp16 2'-*O*-MTase by nsp10 is universal to
457 coronaviruses including FCoV (Figs. 1 and 4). In contrast with the nsp16 of other
458 coronaviruses, FCoV nsp16 possesses a low but detectable 2'-*O*-MTase activity but it
459 is stimulated to full activity by its cognate nsp10 (Fig. 1)
460 Interestingly, the nsp10s of coronaviruses could activate and stimulate, in varying
461 degrees, the 2'-*O*-MTase activities of non-cognate nsp16s except that of IBV
462 (*gammacoronavirus*) (Fig. 4), indicating that both nsp10 and nsp16 have been
463 structurally and functionally conserved during coronavirus evolution. Moreover, the

strength of the nsp16 2'-*O*-MTase activity stimulated by non-cognate nsp10 corresponds to the phylogenetic distances and taxonomic positions of nsp10 and nsp16 in their phylogenetic trees, in which *alphacoronavirus* is more closely related to *betacoronavirus* (data not shown). However, in the phylogenetic tree inferred using genome RNA, *gammacoronavirus* is more closely related to *betacoronavirus*, indicating that nsp10 has coevolved with nsp16 at the protein level. Furthermore, the nsp10 mutants of IBV (K to A and F to A indicated by open triangles in Fig. 3A) showed the weakest stimulation capability of 2'-*O*-MTase comparing with other coronaviruses (Fig. 5A). These results indicate that the stimulation of IBV (*gammacoronaviral*) 2'-*O*-MTase activity most strictly depends on the assistance of its cognate nsp10, and the two critical residues of IBV nsp10 are essential for the interaction of the nsp10/nsp16 complex. Therefore, although MHV nsp10 cannot stimulate IBV nsp16, the interaction domain of MHV nsp10 that contains the two critical residues and is 4 amino acids shorter than the corresponding interaction region of IBV nsp10 (Fig. 3A), could still possess the capability to bind with nsp16 of IBV. Such an assumption was supported by our result that the peptide P29 that is derived from the interaction domain of MHV nsp10 could strongly suppress the 2'-*O*-MTase activity of IBV (Fig. 5B). The conserved mechanism and the interchangeability of nsp10 in stimulating nsp16 provide a theoretical basis for possible development of broad-spectrum inhibitors by targeting coronaviral nsp10/nsp16 2'-*O*-MTase (Fig. 6).

During coronavirus replication, ORF1b (harboring nsp16) is translated via a -1 ribosomal frameshifting mechanism from ORF1a that contains nsp10 (42) , and

Journal of Virology

consequently nsp10 is produced in 3 to 5 fold excess relative to nsp16 in infected cells (35, 36). Although nsp10 and nsp16 exist at 1:1 ratio in the crystal structure (27, 28), we demonstrate that the surplus nsp10 could significantly increase the enzymatic activity of nsp16 (Fig. 2). Moreover, the critical residues of nsp10s (K/R and F/Y are indicated by open triangles in Fig. 3A), which are essential for the stimulation of 2'-*O*-MTase activities of coronaviruses (Fig. 5A), are concentrated in the interaction region of around 42 amino acids. In contrast, the conserved residues of nsp16s involved in the interaction of nsp10/nsp16 complex are scattered throughout a large region of the protein and brought together to the interface by protein folding (28, 30). Therefore, it is more feasible to design inhibitory peptides by mimicking the sequence of the interaction interface of nsp10 rather than nsp16. Comparing with the MTase inhibitors previously used in research work, the peptide inhibitor developed based on the characteristics of coronaviruses 2'-*O*-MTases could more specifically repress viral replication without less side effects (Figs. 6 and 7) because it specifically targets the viral structure that does not exist in cellular proteins.

Previous studies have revealed that the viral RNA cap structures play important roles in viral replication, evasion of recognition by host RNA sensors and suppression of IFN-mediated antiviral response (6, 7). Therefore, antiviral drugs targeting the viral RNA capping enzymes may lead to both inhibition of virus replication and enhancement of interferon responses as we demonstrated in this study (Fig. 7). It is interesting that the inhibitory efficiency of TP29 was remarkably higher in vivo in animal infection than that in biochemical assays and cell culture. This may be

explained by the enhancement of antiviral response *in vivo* when the 2'-*O*-MTase activity is inhibited by the peptide. Many studies have reported that coronaviruses are poor inducers of type I IFN in cell lines (43). However, in primary cells such as plasmacytoid dendritic cells (pDC) and macrophages, IFN is induced by MHV infection (33, 44, 45). In this study, we assume that TP29 treatment may have suppressed the 2'-*O*-MTase activity of nsp10/nsp16, which may lead to increase of the blood level of IFN-β at the early stage of infection and consequently enhance the antiviral immunity in animals. Here, we propose a testable hypothesis to explain how the peptide inhibitor promotes antiviral response and suppresses virus replication (Fig. 8). First, the peptide may inhibit the formation nsp10/nsp16 complex and the 2'-*O*-MTase activity, directly contributing to the suppression of genome replication; second, the reduced 2'-*O*-MTase activity of nsp16 may lead to deficiency in the 2'-*O*-methylation in the RNA cap structure, thus resulting in more cap-0 structures, which have a lower efficiency of translation and consequently suppress the synthesis of viral proteins, and third, the viral RNA lacking a cap-1 structure can be recognized by innate RNA sensors and thus stimulate the type I interferon responses (Fig. 8). These possibilties shall be tested in the future studies to reveal the mechanisms of peptide-mediated inhibition of coronavirus replication.

In conclusion, our data demonstrate that stimulation of nsp16 2'-*O*-MTase activity by nsp10 is a common mechanism for coronaviruses, and nsp10 is functionally interchangeable in activation and stimulation of non-cognate nsp16 among different coronaviruses. Moreover, broad-spectrum inhibitors can be developed by targeting the

nsp10/nsp16 2'-*O*-MTase as demonstrated by the result that the MHV nsp10-derived TP29 peptide can suppress 2'-*O*-MTase activity of different coronaviruses and efficiently suppress MHV-induced pathogenesis in mice by promoting antiviral responses. Therefore, our study provides experimental evidence and the proof-of-principle that peptide inhibitor targeting the 2'-*O*-MTase can efficiently suppress coronavirus replication, suggesting that the 2'-*O*-MTases of coronaviruses may be ideal and potential antiviral drug targets. In future work, more potent peptides will be screened and optimized to inhibit the 2'-*O*-MTase activity and replication of coronaviruses.

Acknowledgments

We thank Dr. Eric J. Snijder for kindly providing the expression plasmids for IBV nsp16 and nsp10 (pDest14-IBV-nsp16 and pDest14-IBV-nsp10), Dr. Peter J. M. Rottier for the FCoV cDNA and Dr. Rong Ye for MHV strain A59 and L2 cells. We are grateful to Dr. Luis. Enjuanes for providing the TGEV cDNA and SARS-CoV replicon.

This research was supported by the China "973" Basic Research Program (2013CB911101), China NSFC grants (81130083, 81271817, 31170152 and 31221061), Wuhan Science and Technology Project (2014060101010055), and Sigrid Juselius Foundation.

References

1. Furuichi, Y., and A. J. Shatkin. 2000. Viral and cellular mRNA capping: past and

prospects. Advances in virus research 55:135-184.

2. Liu, H., and M. Kiledjian. 2006. Decapping the message: a beginning or an end. Biochem Soc Trans 34:35-38.

3. Pichlmair, A., O. Schulz, C. P. Tan, T. I. Naslund, P. Liljestrom, F. Weber, and C. Reis e Sousa. 2006. RIG-I-mediated antiviral responses to single-stranded RNA bearing 5'-phosphates. Science 314:997-1001.

4. Hornung, V., J. Ellegast, S. Kim, K. Brzozka, A. Jung, H. Kato, H. Poeck, S. Akira, K. K. Conzelmann, M. Schlee, S. Endres, and G. Hartmann. 2006. 5'-Triphosphate RNA is the ligand for RIG-I. Science 314:994-997.

5. Ray, D., A. Shah, M. Tilgner, Y. Guo, Y. Zhao, H. Dong, T. S. Deas, Y. Zhou, H. Li, and P. Y. Shi. 2006. West Nile virus 5'-cap structure is formed by sequential guanine N-7 and ribose 2'-O methylations by nonstructural protein 5. J Virol 80:8362-8370.

6. Zust, R., L. Cervantes-Barragan, M. Habjan, R. Maier, B. W. Neuman, J. Ziebuhr, K. J. Szretter, S. C. Baker, W. Barchet, M. S. Diamond, S. G. Siddell, B. Ludewig, and V. Thiel. 2011. Ribose 2'-O-methylation provides a molecular signature for the distinction of self and non-self mRNA dependent on the RNA sensor Mda5. Nature immunology 12:137-143.

7. Daffis, S., K. J. Szretter, J. Schriewer, J. Li, S. Youn, J. Errett, T. Y. Lin, S. Schneller, R. Zust, H. Dong, V. Thiel, G. C. Sen, V. Fensterl, W. B. Klimstra, T. C. Pierson, R. M. Buller, M. Gale, Jr., P. Y. Shi, and M. S. Diamond. 2010. 2'-O methylation of the viral mRNA cap evades host restriction by IFIT family members. Nature 468:452-456.

8. Woyciniuk, P., M. Linder, and C. Scholtissek. 1995. The methyltransferase inhibitor Neplanocin A interferes with influenza virus replication by a mechanism different from

that of 3-deazaadenosine. Virus research 35:91-99.

9. Chrebet, G. L., D. Wisniewski, A. L. Perkins, Q. Deng, M. B. Kurtz, A. Marcy, and S. A. Parent. 2005. Cell-based assays to detect inhibitors of fungal mRNA capping enzymes and characterization of sinefungin as a cap methyltransferase inhibitor. Journal of biomolecular screening 10:355-364.

10. Masters, P. S. 2006. The molecular biology of coronaviruses. Advances in virus research 66:193-292.

11. Li, W., Z. Shi, M. Yu, W. Ren, C. Smith, J. H. Epstein, H. Wang, G. Crameri, Z. Hu, H. Zhang, J. Zhang, J. McEachern, H. Field, P. Daszak, B. T. Eaton, S. Zhang, and L. F. Wang. 2005. Bats are natural reservoirs of SARS-like coronaviruses. Science 310:676-679.

12. Lau, S. K., P. C. Woo, K. S. Li, Y. Huang, H. W. Tsoi, B. H. Wong, S. S. Wong, S. Y. Leung, K. H. Chan, and K. Y. Yuen. 2005. Severe acute respiratory syndrome coronavirus-like virus in Chinese horseshoe bats. Proceedings of the National Academy of Sciences of the United States of America 102:14040-14045.

13. Ge, X. Y., J. L. Li, X. L. Yang, A. A. Chmura, G. Zhu, J. H. Epstein, J. K. Mazet, B. Hu, W. Zhang, C. Peng, Y. J. Zhang, C. M. Luo, B. Tan, N. Wang, Y. Zhu, G. Crameri, S. Y. Zhang, L. F. Wang, P. Daszak, and Z. L. Shi. 2013. Isolation and characterization of a bat SARS-like coronavirus that uses the ACE2 receptor. Nature 503:535-538.

14. Martina, B. E., B. L. Haagmans, T. Kuiken, R. A. Fouchier, G. F. Rimmelzwaan, G. Van Amerongen, J. S. Peiris, W. Lim, and A. D. Osterhaus. 2003. Virology: SARS virus infection of cats and ferrets. Nature 425:915.

15. de Groot, R. J., S. C. Baker, R. S. Baric, C. S. Brown, C. Drosten, L. Enjuanes, R. A.

595 Fouchier, M. Galiano, A. E. Gorbalenya, Z. A. Memish, S. Perlman, L. L. Poon, E. J.
596 Snijder, G. M. Stephens, P. C. Woo, A. M. Zaki, M. Zambon, and J. Ziebuhr. 2013.
597 Middle East respiratory syndrome coronavirus (MERS-CoV): announcement of the
598 Coronavirus Study Group. Journal of virology 87:7790-7792.
599 16. Gorbalenya, A. E., E. J. Snijder, and W. J. Spaan. 2004. Severe acute respiratory
600 syndrome coronavirus phylogeny: toward consensus. J Virol 78:7863-7866.
601 17. Brierley, I., P. Digard, and S. C. Inglis. 1989. Characterization of an efficient coronavirus
602 ribosomal frameshifting signal: requirement for an RNA pseudoknot. Cell 57:537-547.
603 18. te Velthuis, A. J., J. J. Arnold, C. E. Cameron, S. H. van den Worm, and E. J. Snijder.
604 2010. The RNA polymerase activity of SARS-coronavirus nsp12 is primer dependent.
605 Nucleic acids research 38:203-214.
606 19. Imbert, I., J. C. Guillemot, J. M. Bourhis, C. Bussetta, B. Coutard, M. P. Egloff, F. Ferron,
607 A. E. Gorbalenya, and B. Canard. 2006. A second, non-canonical RNA-dependent RNA
608 polymerase in SARS coronavirus. The EMBO journal 25:4933-4942.
609 20. Ivanov, K. A., V. Thiel, J. C. Dobbe, Y. van der Meer, E. J. Snijder, and J. Ziebuhr. 2004.
610 Multiple enzymatic activities associated with severe acute respiratory syndrome
611 coronavirus helicase. Journal of virology 78:5619-5632.
612 21. Minskaia, E., T. Hertzig, A. E. Gorbalenya, V. Campanacci, C. Cambillau, B. Canard,
613 and J. Ziebuhr. 2006. Discovery of an RNA virus 3'->5' exoribonuclease that is critically
614 involved in coronavirus RNA synthesis. Proceedings of the National Academy of Sciences
615 of the United States of America 103:5108-5113.
616 22. Chen, P., M. Jiang, T. Hu, Q. Liu, X. S. Chen, and D. Guo. 2007. Biochemical

characterization of exoribonuclease encoded by SARS coronavirus. Journal of biochemistry and molecular biology 40:649-655.

23. Chen, Y., H. Cai, J. Pan, N. Xiang, P. Tien, T. Ahola, and D. Guo. 2009. Functional screen reveals SARS coronavirus nonstructural protein nsp14 as a novel cap N7 methyltransferase. Proceedings of the National Academy of Sciences of the United States of America 106:3484-3489.

24. Ivanov, K. A., T. Hertzig, M. Rozanov, S. Bayer, V. Thiel, A. E. Gorbalenya, and J. Ziebuhr. 2004. Major genetic marker of nidoviruses encodes a replicative endoribonuclease. Proceedings of the National Academy of Sciences of the United States of America 101:12694-12699.

25. Decroly, E., I. Imbert, B. Coutard, M. Bouvet, B. Selisko, K. Alvarez, A. E. Gorbalenya, E. J. Snijder, and B. Canard. 2008. Coronavirus nonstructural protein 16 is a cap-0 binding enzyme possessing (nucleoside-2'O)-methyltransferase activity. Journal of virology 82:8071-8084.

26. Bouvet, M., C. Debarnot, I. Imbert, B. Selisko, E. J. Snijder, B. Canard, and E. Decroly. 2010. In vitro reconstitution of SARS-coronavirus mRNA cap methylation. PLoS pathogens 6:e1000863.

27. Decroly, E., C. Debarnot, F. Ferron, M. Bouvet, B. Coutard, I. Imbert, L. Gluais, N. Papageorgiou, A. Sharff, G. Bricogne, M. Ortiz-Lombardia, J. Lescar, and B. Canard. 2011. Crystal structure and functional analysis of the SARS-coronavirus RNA cap 2'-O-methyltransferase nsp10/nsp16 complex. PLoS pathogens 7:e1002059.

28. Chen, Y., C. Su, M. Ke, X. Jin, L. Xu, Z. Zhang, A. Wu, Y. Sun, Z. Yang, P. Tien, T. Ahola,

Y. Liang, X. Liu, and D. Guo. 2011. Biochemical and structural insights into the mechanisms of SARS coronavirus RNA ribose 2'-O-methylation by nsp16/nsp10 protein complex. PLoS pathogens 7:e1002294.

29. Chen, Y., J. Tao, Y. Sun, A. Wu, C. Su, G. Gao, H. Cai, S. Qiu, Y. Wu, T. Ahola, and D. Guo. 2013. Structure-function analysis of severe acute respiratory syndrome coronavirus RNA cap guanine-N7-methyltransferase. Journal of virology 87:6296-6305.

30. Ke, M., Y. Chen, A. Wu, Y. Sun, C. Su, H. Wu, X. Jin, J. Tao, Y. Wang, X. Ma, J. A. Pan, and D. Guo. 2012. Short peptides derived from the interaction domain of SARS coronavirus nonstructural protein nsp10 can suppress the 2'-O-methyltransferase activity of nsp10/nsp16 complex. Virus research 167:322-328.

31. Jin, X., Y. Chen, Y. Sun, C. Zeng, Y. Wang, J. Tao, A. Wu, X. Yu, Z. Zhang, J. Tian, and D. Guo. 2013. Characterization of the guanine-N7 methyltransferase activity of coronavirus nsp14 on nucleotide GTP. Virus research 176:45-52.

32. Pan, J., X. Peng, Y. Gao, Z. Li, X. Lu, Y. Chen, M. Ishaq, D. Liu, M. L. Dediego, L. Enjuanes, and D. Guo. 2008. Genome-wide analysis of protein-protein interactions and involvement of viral proteins in SARS-CoV replication. PloS one 3:e3299.

33. Roth-Cross, J. K., S. J. Bender, and S. R. Weiss. 2008. Murine coronavirus mouse hepatitis virus is recognized by MDA5 and induces type I interferon in brain macrophages/microglia. Journal of virology 82:9829-9838.

34. Yang, J., Z. Sun, Y. Wang, J. Lv, D. Qu, and R. Ye. 2011. Partial deletion in the spike endodomain of mouse hepatitis virus decreases the cytopathic effect but maintains foreign protein expression in infected cells. Journal of virological methods 172:46-53.

35. Egloff, M. P., F. Ferron, V. Campanacci, S. Longhi, C. Rancurel, H. Dutartre, E. J. Snijder, A. E. Gorbalenya, C. Cambillau, and B. Canard. 2004. The severe acute respiratory syndrome-coronavirus replicative protein nsp9 is a single-stranded RNA-binding subunit unique in the RNA virus world. Proceedings of the National Academy of Sciences of the United States of America 101:3792-3796.

36. Thiel, V., K. A. Ivanov, A. Putics, T. Hertzig, B. Schelle, S. Bayer, B. Weissbrich, E. J. Snijder, H. Rabenau, H. W. Doerr, A. E. Gorbalenya, and J. Ziebuhr. 2003. Mechanisms and enzymes involved in SARS coronavirus genome expression. The Journal of general virology 84:2305-2315.

37. Lugari, A., S. Betzi, E. Decroly, E. Bonnaud, A. Hermant, J. C. Guillemot, C. Debarnot, J. P. Borg, M. Bouvet, B. Canard, X. Morelli, and P. Lecine. 2010. Molecular mapping of the RNA Cap 2'-O-methyltransferase activation interface between severe acute respiratory syndrome coronavirus nsp10 and nsp16. The Journal of biological chemistry 285:33230-33241.

38. Piantavigna, S., G. A. McCubbin, S. Boehnke, B. Graham, L. Spiccia, and L. L. Martin. 2011. A mechanistic investigation of cell-penetrating Tat peptides with supported lipid membranes. Biochimica et biophysica acta 1808:1811-1817.

39. Battegay, M., S. Cooper, A. Althage, J. Banziger, H. Hengartner, and R. M. Zinkernagel. 1991. Quantification of lymphocytic choriomeningitis virus with an immunological focus assay in 24- or 96-well plates. Journal of virological methods 33:191-198.

40. van Hemert, M. J., S. H. van den Worm, K. Knoops, A. M. Mommaas, A. E. Gorbalenya, and E. J. Snijder. 2008. SARS-coronavirus replication/transcription complexes are

membrane-protected and need a host factor for activity in vitro. PLoS pathogens 4:e1000054.

41. Gosert, R., A. Kanjanahaluethai, D. Egger, K. Bienz, and S. C. Baker. 2002. RNA replication of mouse hepatitis virus takes place at double-membrane vesicles. Journal of virology 76:3697-3708.

42. Snijder, E. J., P. J. Bredenbeek, J. C. Dobbe, V. Thiel, J. Ziebuhr, L. L. Poon, Y. Guan, M. Rozanov, W. J. Spaan, and A. E. Gorbalenya. 2003. Unique and conserved features of genome and proteome of SARS-coronavirus, an early split-off from the coronavirus group 2 lineage. Journal of molecular biology 331:991-1004.

43. Roth-Cross, J. K., L. Martinez-Sobrido, E. P. Scott, A. Garcia-Sastre, and S. R. Weiss. 2007. Inhibition of the alpha/beta interferon response by mouse hepatitis virus at multiple levels. Journal of virology 81:7189-7199.

44. Cervantes-Barragan, L., R. Zust, F. Weber, M. Spiegel, K. S. Lang, S. Akira, V. Thiel, and B. Ludewig. 2007. Control of coronavirus infection through plasmacytoid dendritic-cell-derived type I interferon. Blood 109:1131-1137.

45. Cervantes-Barragan, L., U. Kalinke, R. Zust, M. Konig, B. Reizis, C. Lopez-Macias, V. Thiel, and B. Ludewig. 2009. Type I IFN-mediated protection of macrophages and dendritic cells secures control of murine coronavirus infection. J Immunol 182:1099-1106.

Figure Legend

Fig. 1. Biochemical analysis of the 2'-*O*-MTase activity of coronavirus proteins. (A) The SDS-PAGE of the recombinant nsp16 and nsp10 of 6 coronaviruses. (B to G)

705 Purified nsp10 (18 μM) and nsp16 (3.0 μM) of the indicated coronaviruses were
706 incubated with the substrate m7GpppA-RNA (with a cap-0 structure at the 5'-end) in
707 the presence of [^{3}H]-AdoMet. The 2'-*O*-MTase activities were analyzed by liquid
708 scintillation assays after purification of the ^{3}H-labeled substrates with
709 DEAE-Sephadex chromatography. SARS-CoV nsp7 and vaccinia virus 2'-*O*-MTase
710 (VP39) were used as a negative and positive control, respectively (n = 3, mean values
711 ± SD). ***p < 0.001 (unpaired Students's t-test). (H) TLC analysis of nuclease
712 P1-resistant cap structures released from ^{32}P-labeled m7G*pppA-RNA methylated by
713 nsp16 or nsp10/nsp16 complex of TGEV, FCoV, MHV, SARS-CoV, MERS-CoV and
714 IBV, respectively. The markers G*pppA, m7G*pppA, and m7G*pppAm were
715 prepared with commercial vaccinia virus capping enzymes. The position of origin and
716 migration of G*pppA, m7G*pppA, and m7G*pppAm are indicated on the left.
717 SARS-CoV nsp7, vaccinia virus N7-MTase (D1-D12) and 2'-*O*-MTase (VP39) were
718 used as a negative and positive control, respectively.

719 **Fig. 2. MTase assays of coronavirus nsp16 with different molar ratios of cognate**
720 **nsp10.** The substrate m^{7}GpppA-RNAs with a cap-0 structure were used to test the
721 2'-*O*-MTase activities of nsp16 of TGEV, FCoV, SARS-CoV and IBV. The ratio of
722 nsp10 to nsp16 is indicated below the x-axis (n = 3, mean values ± SD).

723 **Fig. 3. Conservation of nsp10 and nsp16 in coronaviruses.** (A and B) Primary
724 sequence alignments of nsp10 (A) and nsp16 (B) of TGEV, FCoV, MHV, SARS-CoV,
725 MERS-CoV and IBV. The well conserved and relatively conserved residues are
726 indicated by solid black boxes and solid gray boxes, respectively. The conserved

residues invovled in the interactions of nsp10/nsp16 complexes are indicated by solid black and open triangles. The region corresponding to the peptide inhibitor P29 is marked by a line indicates. The aligment was generated with the program Clustal and the figure was prepared using Genedoc. (C and D) MTase assays of *alphacoronaviral* nsp16 (C) and *betacoronaviral* nsp16 (D) stimulated by the non-cognate nsp10 from a coronavirus of the same generus. SARS-CoV nsp7 and vaccinia virus 2'-*O*-MTase (VP39) were used as a negative and positive control, respectively (n = 3, mean values ± SD).

Fig. 4. MTase assays of nsp16 stimulated by non-cognate nsp10 from different genera of coronaviruses. The m7GpppA-RNAs with a cap-0 structure were used to test the 2'-*O*-MTase activities of nsp16 of TGEV (A), FCoV (B), MHV (C), SARS-CoV (D), MERS-CoV (E) and IBV (F) stimulated by nsp10 from different genera of coronaviruses as indicated. SARS-CoV nsp7 and vaccinia virus 2'-*O*-MTase (VP39) were used as a negative and positive control, respectively (n = 3, mean values ± SD). ***p < 0.001 and no significant (ns) (unpaired Students's t-test).

Fig. 5. Biochemical analyses of nsp10 mutants and its derived short peptides. (A) The MTase activities of nsp16 of TGEV, FCoV, MHV, SARS-CoV, MERS-CoV and IBV, stimulated by corresponding wild type nsp10 and their mutants K/R to A or F/Y to A, were tested by MTase assays. (B) The inhibition effects of P29, P29M and P29S peptides at a final concentration of 200 μM on 2'-*O*-MTase activities of different coronaviruses (n = 3, mean values ± SD). ***p < 0.001 (unpaired Students's t-test).

748 **Fig. 6. Inhibitory effects of short peptides on coronavirus replications in cell**
749 **culture models.** (A) and (B) The inhibitory effects of the peptides TP29, TP29M, P29
750 and TP29S at the final concentration of 200 μM and PBS control on the replication of
751 MHV-A59 in L2 cells. The virus titers were determined by Virus Counter (A) and
752 further comfirmed by the plaque assays in L2 cells 20 hr post infection (B). (C) The
753 plaque size of MHV-A59 on L2 cells with treatment of TP29S or TP29 at the final
754 concentration of 200 μM. (D) Inhibition effects of TP29 at different final
755 concentration (0-800 μM) on the replication of MHV-A59. (E) The inhibitory effects
756 of the indicated peptides on the replication of SARS-CoV replicon. (n = 3, mean
757 values ± SD). *$p < 0.05$, **$p < 0.01$, ***$p<0.001$ and not significant (ns) (unpaired
758 Students's t-test).

759 **Fig. 7. Rescue of MHV infected mice by peptide inhibitor TP29.** (A) Lethality of
760 groups of MHV-infected or mock-treated mice (n = 10) after treatment with peptides
761 (PBS, TP29 and TP29S). The mice were monitored for 14 days. (B and C) Viral titers
762 of clarified liver homogenates (B) and serum ALT (alanine aminotransferase) values
763 (C) were determined at day 3 postinfection. 0 hr or 1hr represents that peptides were
764 injected immediately or 1 hour after the mice (n = 7) were infected with MHV-A59.
765 The virus titer was normalized for liver mass. (D) Enzyme-linked immunosorbent
766 assay of interferon-β in serum 12 h, 24 h and 72 h post infection with MHV-A59 and
767 injection of 0.05 mg/g (amount of peptide to body weight of mice) TP29 or TP29S
768 peptide (n = 7). V represents MHV infection; B = PBS, P = TP29 and S = TP29S
769 (scrambled TP29). TP29 injection without MHV infection (P) was used as mock

control. Viral titers (E) and serum ALT values (F) were measured at the indicated time points. Groups of mice (n = 7) were sacrificed at 1, 3, 5 and 7 days p.i. (G) Hematoxylin and eosin stainingof paraformaldehyde-fixed liver sections at day 1, 3, 5 and 7 p.i of C57BL/6 mice (magnification, x40; inset, x200). (n = 7, mean values ± SD), *p< 0.05, **p < 0.01, ***p < 0.001 and not significant (ns) (unpaired Students's t-test).

Fig. 8. Hypothesis for the mechanisms of peptide TP29-mediated inhibition of coronavirus infection. Peptide inhibitor TP29 may modulate three steps in the coronavirus replication cycle: inhibiting the formation of nsp10/nsp16 complex, decreasing the translation efficiency of viral RNAs, and promoting the recognition of viral RNAs by cellular innate RNA sensors, leading to enhanced immune responses.

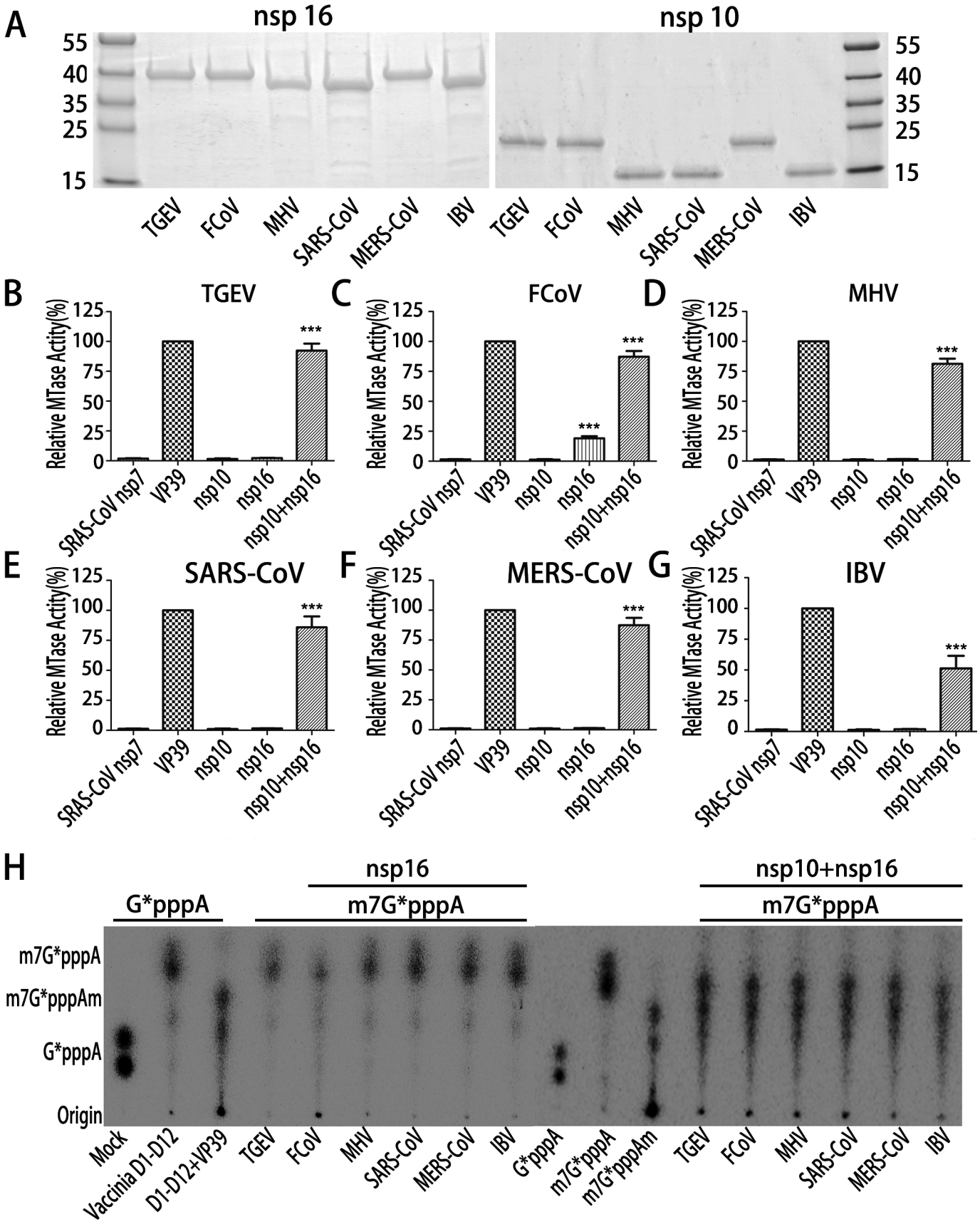

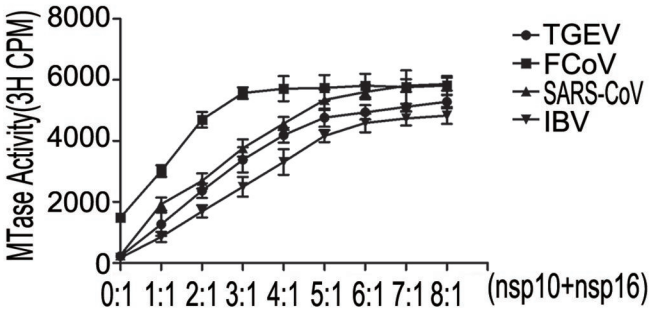

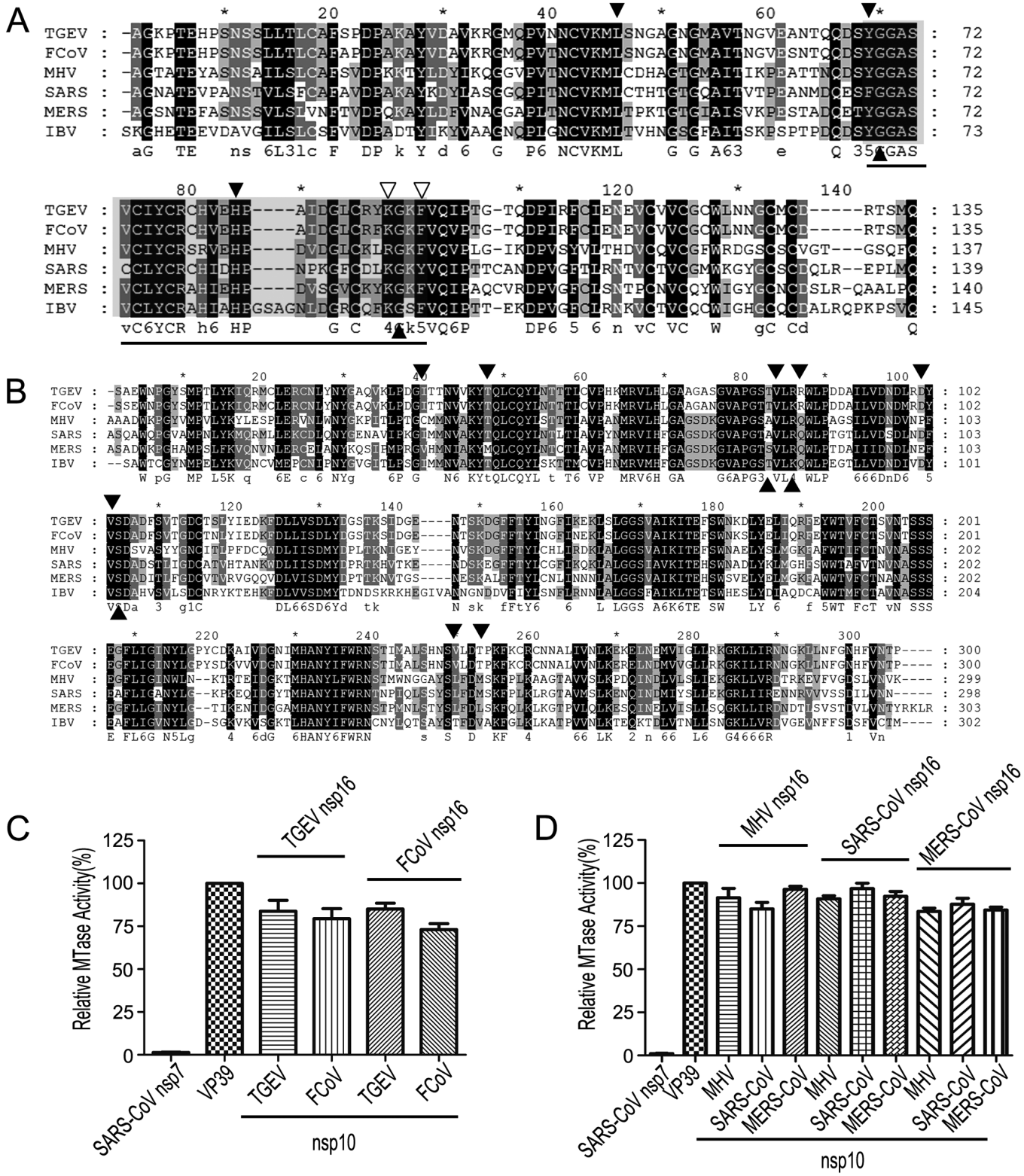

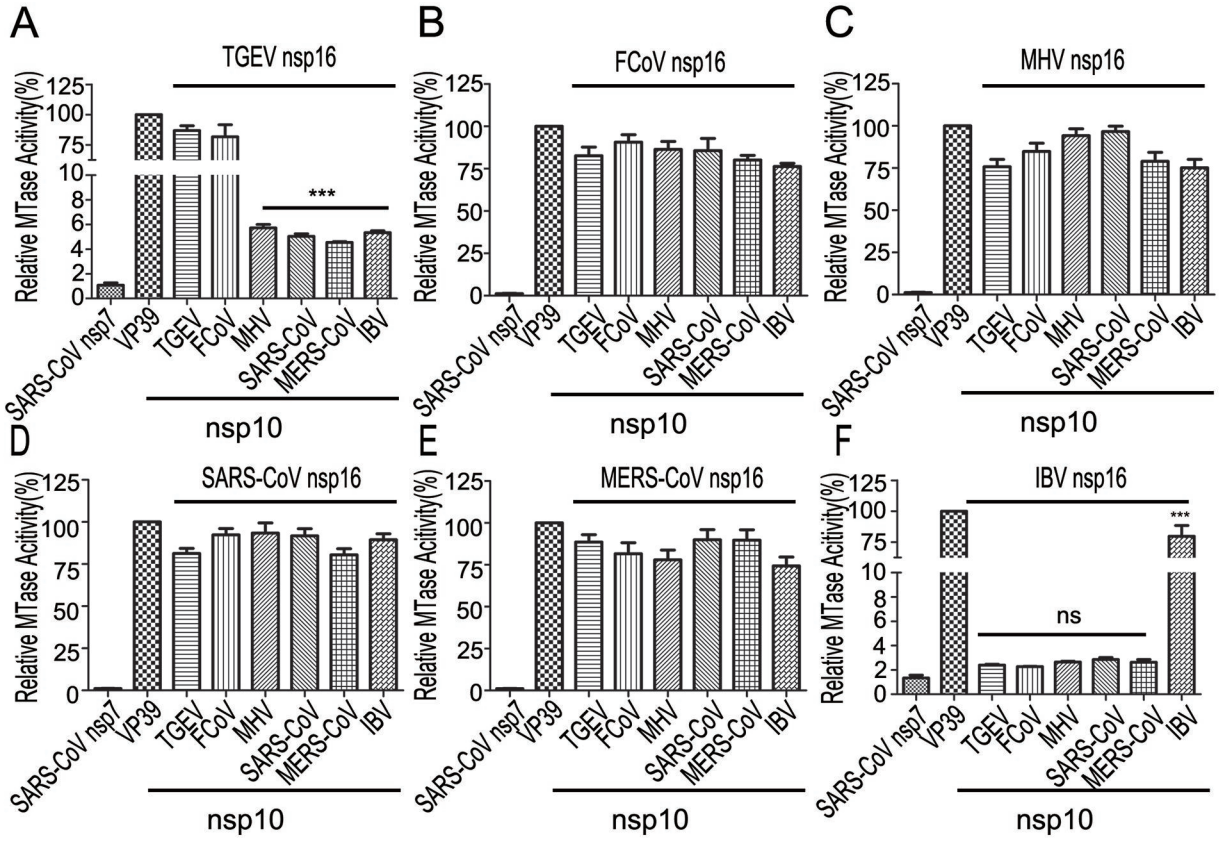

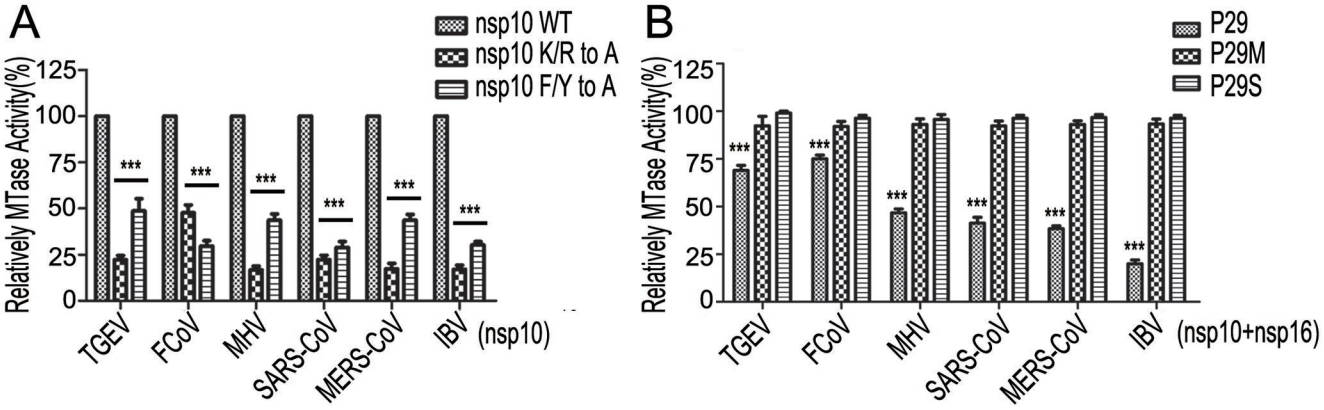

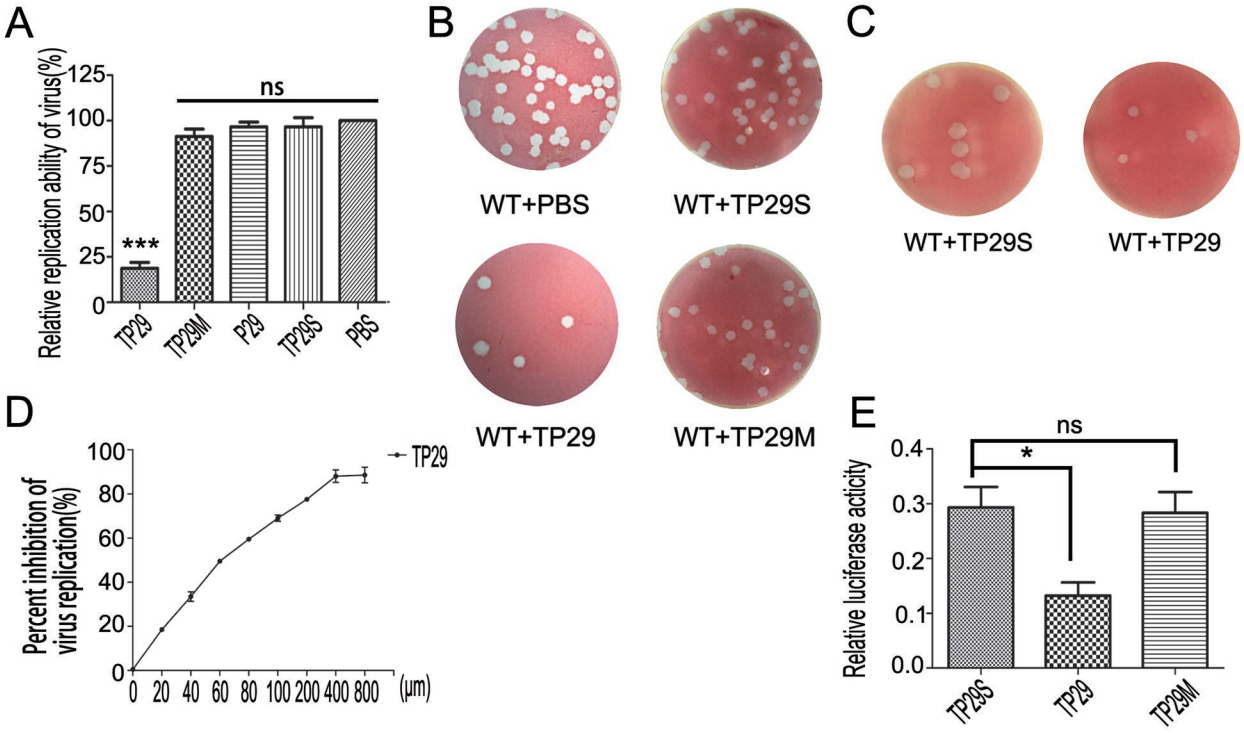

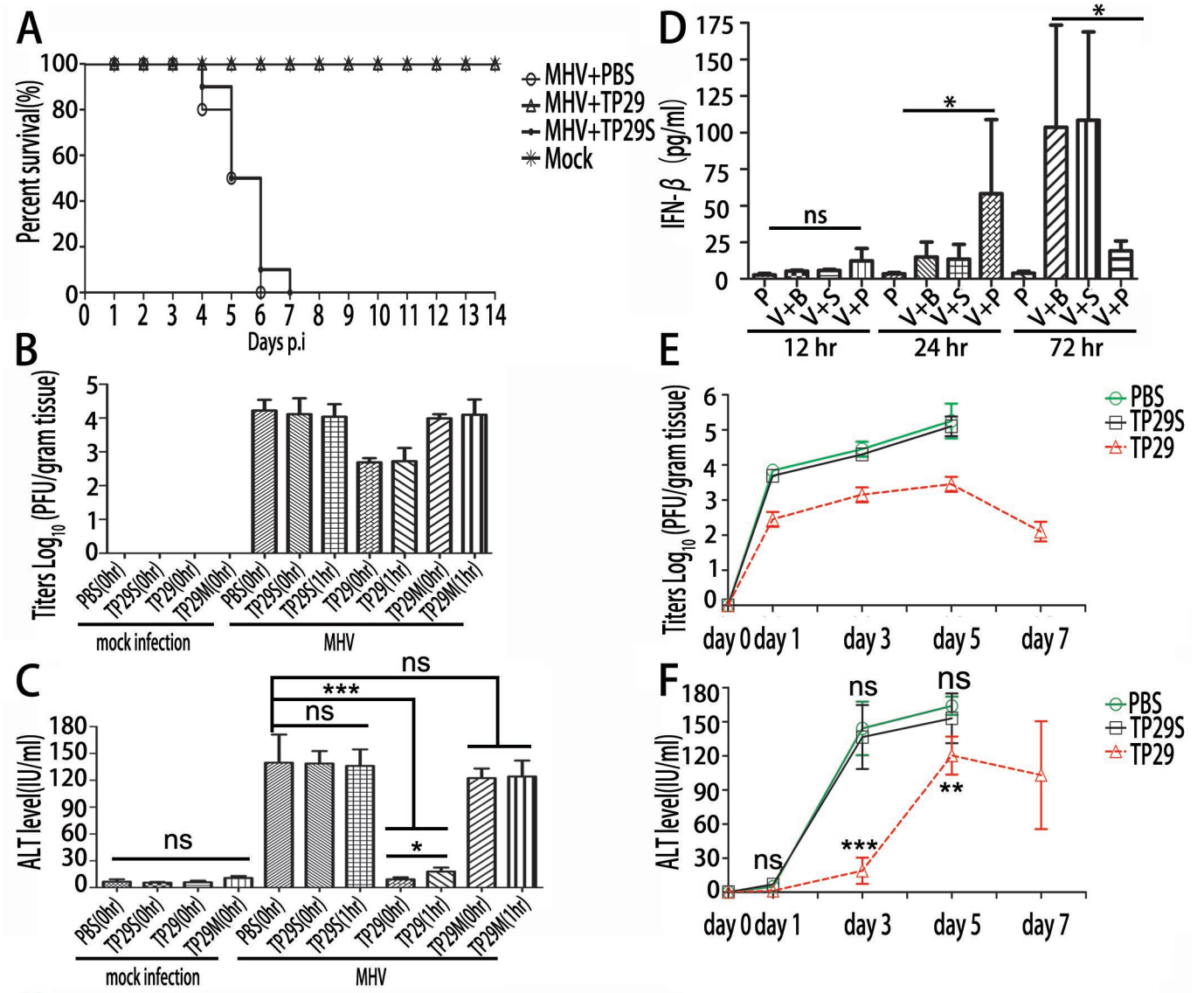

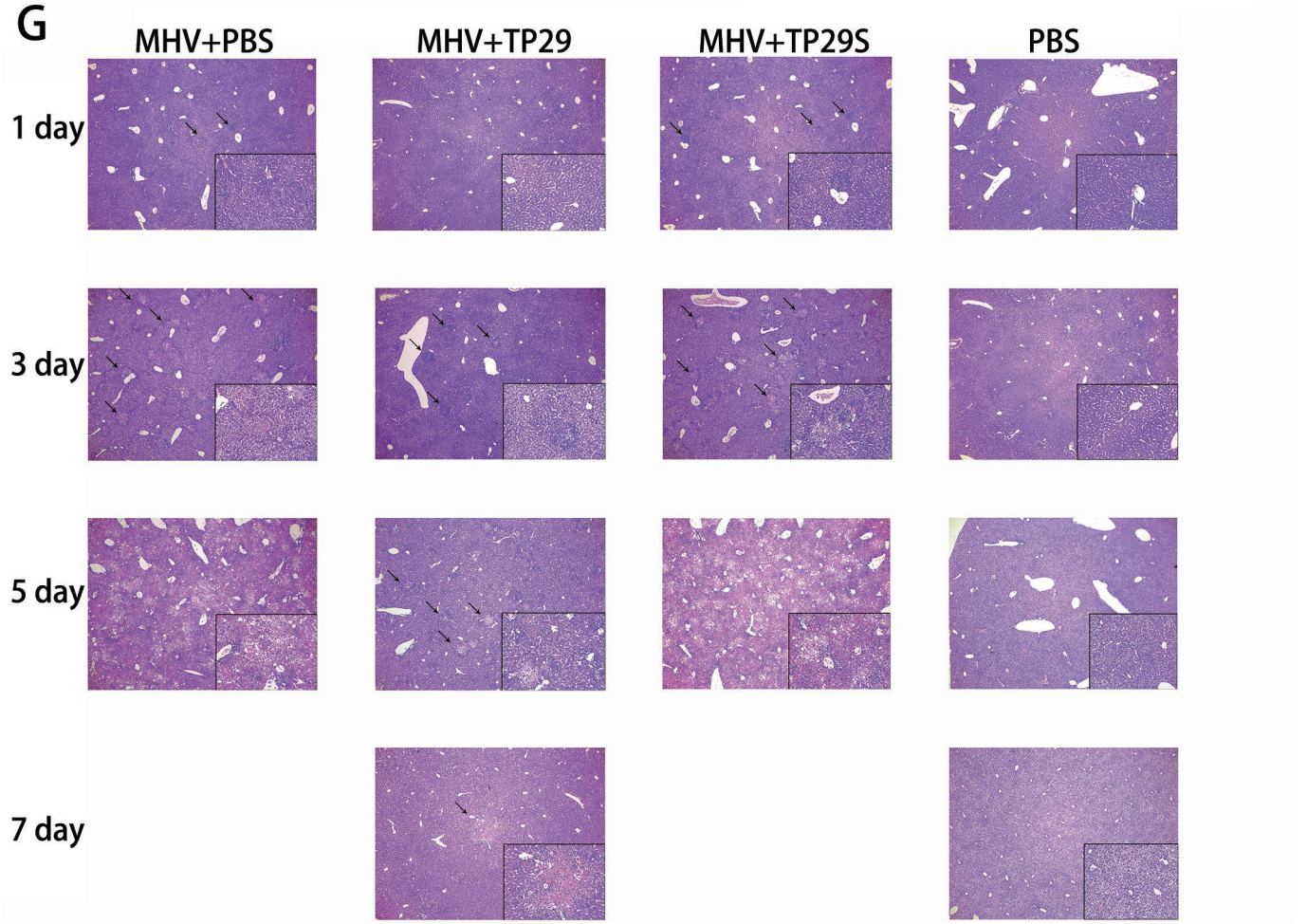

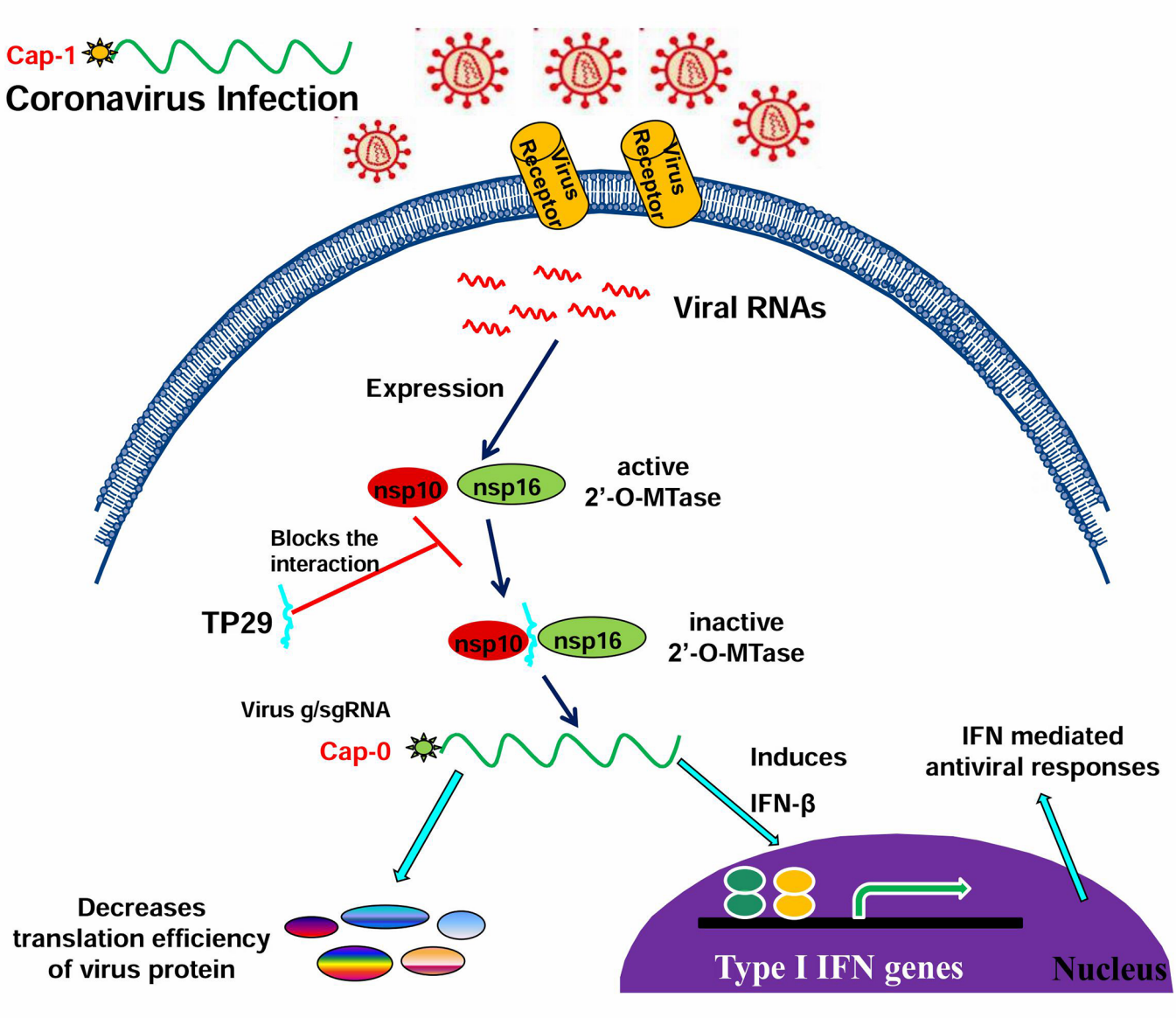

Table 1. List of short peptides designed based on MHV nsp10

Peptides	**Amino acid sequences**[a]
P29	YGGASVCIYCRSRVEHPDVDGLCKLRGKF
P29M (P29-R93A&Y96A)	YGGASVCIYCRSRVEHPDVDGLCKLAGKA
P29S (scrambled P29)	VLKLSCCYDGYIRACSRVGEPVGGSDDFH
TP29 (Tat-P29)	*YGRKKRRQRRRGSG*YGGASVCIYCRSRVEHPDVDGLCKLRGKF
TP29M (Tat-P29-R93A&Y96A)	*YGRKKRRQRRRGSG*YGGASVCIYCRSRVEHPDVDGLCKLAGKA
TP29S (Tat-Scramble P29)	*YGRKKRRQRRRGSG*VLKLSCCYDGYIRACSRVGEPVGGSDDFH

[a] Italics indicates the sequence of HIV-Tat.